GEOPHYSICS, VOL. 68, NO. 5 (SEPTEMBER-OCTOBER 2003); P. 1592–1599, 7 FIGS., 4 TABLES.
10.1190/1.1620633

Discrimination between pressure and fluid saturation changes from marine multicomponent time-lapse seismic data

Martin Landrø*, Helene Hafslund Veire*, Kenneth Duffaut‡, and Nazih Najjar**

ABSTRACT

Explicit expressions for computation of saturation and pressure-related changes from marine multicomponent time-lapse seismic data are presented. Necessary input is PP and PS stacked data for the baseline seismic survey and the repeat survey. Compared to earlier methods based on PP data only, this method is expected to be more robust since two independent measurements are used in the computation. Due to a lack of real marine multicomponent time-lapse seismic data sets, the methodology is tested on synthetic data sets, illustrating strengths and weaknesses of the proposed technique. Testing ten scenarios for various changes in pore pressure and fluid saturation, we find that it is more robust for most cases to use the proposed 4D PP/PS technique instead of a 4D PP amplitude variation with offset (AVO) technique. The fit between estimated and "real" changes in water saturation and pore pressure were good for most cases. On the average, we find that the deviation in estimated saturation changes is 8% and 0.3 MPa for the estimated pore pressure changes. For PP AVO, we find that the corresponding average errors are 9% and 1.0 MPa. In the present method, only 4D PP and PS amplitude changes are used in the calculations. It is straightforward to include use of 4D traveltime shifts in the algorithm and, if reliable time shifts can be measured, this will most likely further stabilize the presented method.

INTRODUCTION

Prediction of overpressured zones from seismic data have been tested and reported by several researchers (e.g., Reynolds, 1970; Bilgeri and Ademeno, 1982). The basic tool in such studies has been velocity analysis. By detecting areas where the estimated velocities deviate from the expected compaction trend (velocity increase versus depth), potential overpressure regions are identified by anomalous velocity decreases. For reservoir monitoring purposes, however, this approach is not appropriate for two reasons. First, for normal reservoir depths (2000 m and deeper), conventional velocity analysis is not sufficiently accurate to determine pore pressure changes of 5–6 MPa (or lower, see Kvam and Landrø, 2001). Second, when pore pressure changes and fluid saturation changes are both present, it is impossible to discriminate between the two from P-wave velocity analysis only. In most time-lapse seismic studies, seismic differences between a baseline and a monitor survey are analyzed and interpreted as either a pressure effect or a fluid effect. In the Magnus 4D study (Watts et al., 1996), the main seismic changes were attributed to pore pressure changes, whereas in the Gullfaks (Landrø et al., 1999a) and the Draugen (Gabriels et al., 1999) 4D seismic studies, most of the seismic changes were interpreted as fluid related.

For some fields or segments within a field, both fluid and pressure changes have approximately the same degree of impact on the seismic data. In such cases the use of time-lapse amplitude variation with offset (AVO) analysis offers an opportunity to discriminate between the two effects (Tura and Lumley, 1998, 1999; Landrø, 2001). The major weakness of time-lapse AVO is the lack of seismic repeatability, which influences the quality of the results. As discussed by Cambois (2000), there are many effects that limit precise use of P-wave AVO data, such as wavelet variations with offset, residual multiple energy, residual normal moveout (NMO), etc. For time-lapse AVO, many of these effects are reduced simply because we commit the same error twice and then subtract one from the other. However, for wavelet variations from base to monitor survey (as opposed to wavelet variations with offset), specific matching

Manuscript received by the Editor January 28, 2002; revised manuscript received March 31, 2003.
*Norwegian University of Science & Technology, Department of Petroleum Engineering & Applied Geophysics, N-7491 Trondheim, Norway. E-mail: mlan@ipt.ntnu.no.
‡Statoil Research Centre, Postuttak 7005 Trondheim, Norway.
**Saudi Aramco, P.O. Box 1290, Dharan 31311, Saudi Arabia.

filters should be used. Still, there are major uncertainties associated with time-lapse AVO (Landrø, 2002). This paper shows that the combined use of PP and PS time-lapse seismic data will reduce the overall uncertainty when estimating pressure and saturation changes. Therefore, the main objective of the present paper is to develop and test a methodology for discriminating fluid pressure and saturation changes directly from time-lapse PP and PS seismic stacks.

The technique of acquiring marine multicomponent data was demonstrated by Berg et al. (1994) to image through gas clouds. Since then, multicomponent data has been used for various purposes, as for instance shale-sand discrimination (MacLeod et al., 1999). Landrø et al. (1999b) proposed to use shear-wave elastic impedance as a well calibration tool, and this concept was later tested on a multicomponent data set from Statfjord field (Duffaut et al., 2000).

There are other production-related changes which have impact on time-lapse seismic data (e.g., as gas injection, temperature changes, etc.). In this paper, however, the focus will be on the discrimination between pore pressure and fluid saturation changes. In the following, a method to estimate fluid and pressure-related changes directly from repeated PP and PS partially stacked data will be presented.

SATURATION AND PRESSURE VERSUS SEISMIC PARAMETERS

Distinguishing between fluid saturation and pore pressure changes from seismic data requires knowledge about how seismic parameters are influenced by such changes. In the Gullfaks 4D project (Landrø et al., 1999a) a rock physics model calibrated with well log measurements was used to predict the seismic effect of substituting oil with water. The basic equation in the rock physics modeling is the Gassmann equation (Gassmann, 1951). Repeated logging in wells typically shows a change in water saturation from values around 10% (preproduction) to values around 70–80% (postproduction). The relationship between saturation changes and P-wave velocity after calibrating the Gassmann model to some of the wells at Gullfaks field is shown in Figure 1. A slightly nonlinear relationship is observed. The relationship between seismic parameters and saturation changes can thus be approximated by linear functions to first order at Gullfaks field.

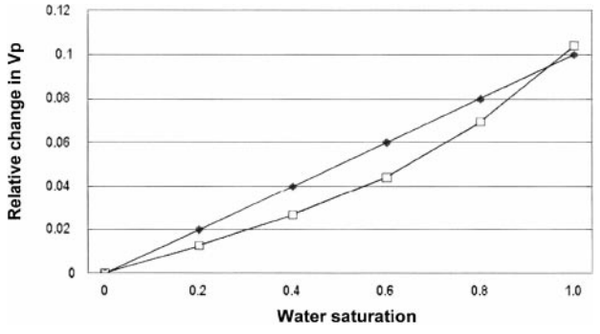

FIG. 1. Typical modeled (Gassmann) relationship between relative change in P-wave velocity and change in water saturation (line with squares). Also shown is the straight line approximation used in the data example (line with diamonds).

A common way to obtain a relationship between seismic parameters and pressure changes is to perform ultrasonic measurements on several cores taken from various formations. A typical curve for P-wave velocity versus effective pressure changes is displayed in Figure 2. This curve represents the average of 29 dry core measurements from Gullfaks field. A similar trend is found for the S-wave velocity versus effective pressure, based on the same 29 plug measurements. The Gullfaks reservoir rock is of early and middle Jurassic age, representing shallow marine to fluvial deposits. The reservoir depth is approximately 2000 m. The initial pore pressure is 32 MPa, and the vertical overburden/external stress is approximately 38 MPa. Typical porosities are around 30%. All measurements were made on dry core samples. Comparison of dry and brine saturated acoustic core measurements shows that the compressional velocities are higher in brine-saturated rock. The saturation effect is more pronounced at lower effective vertical stresses (Winkler, 1985). The effective vertical stress is equal to the vertical stress minus the pore pressure. This means that a pore pressure increase will lead to a decreased effective vertical stress. In comparison with the velocity versus saturation curve shown in Figure 1, the curve in Figure 2 is highly nonlinear. As will be shown later, this nonlinear behavior requires a second order approximation of the relationship between seismic parameters and pressure changes. A summary of the rock physics feasibility study for Gullfaks is shown in Figure 3. To test the proposed algorithm for a variety of pressure-saturation changes, an industrial rock-physics modeling tool (Petrotools) was used (after calibration to the measurements).

The validity of curves such as those shown in Figure 1 and Figure 2 should be discussed. Is it valid to compare velocities measured at high frequencies with seismic velocities? Is it valid to compare pressure measurements made on a dry core sample that has gone through reloading and loading several times with actual stress conditions in the reservoir rock? Despite all these concerns, numerical models obtained from the rock physics study were used as a link between reservoir production changes and seismic changes.

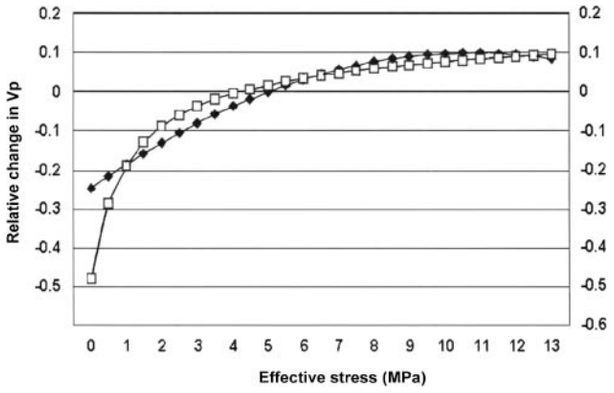

FIG. 2. Relative P-wave velocity change versus change in net effective pressure (line with squares) and the second order approximation used in the data example (line with diamonds). Initial net pressure at Gullfaks is assumed to be around 5–6 MPa, and expected changes in net pressure might range from −5 MPa (for a pore-pressure increase) to +5 MPa (for a pore-pressure decrease).

METHODOLOGY

The methodology is basically an extension of the method presented by Landrø (2001). Consider a two-layer model: a cap rock layer (layer 1, shale) above a reservoir layer (layer 2, sand). For simplicity, the situation when only fluid saturation changes occur in layer 2 will first be studied, next, only pressure changes in layer 2 will be examined. The P-wave velocity in layer 1 (α_1) is assumed to remain constant between the baseline and the repeated survey, as well as for the S-wave velocity (β_1) and the density (ρ_1). In layer 2 (which is assumed to be the porous reservoir layer) the preproduction parameters are denoted α_2, β_2, etc. The same parameters after fluid substitution in layer 2 are denoted $\alpha_2'\beta_2'$, etc. The lithological parameter contrast in P-wave velocity is $\Delta\alpha = \alpha_2 - \alpha_1$, whereas the parameter contrast due to fluid changes in layer 2 can be expressed as $\Delta\alpha^F = \alpha_2' - \alpha_2$, or more precisely;

$$\Delta\alpha^F = \alpha_2[S_W(t_2)] - \alpha_2[S_W(t_1)], \tag{1}$$

where S_W denotes water saturation, t_1 and t_2 denote the timing for the baseline and monitor seismic surveys, respectively, and subscript 2 of α_2, etc. refers to layer 2. The reflection coefficient prior to production is (Aki and Richards, 1980)

$$R_0^{PP}(\theta) = \frac{1}{2}\left(\frac{\Delta\rho}{\rho} + \frac{\Delta\alpha}{\alpha}\right) - \frac{2\beta^2}{\alpha^2}\left(\frac{\Delta\rho}{\rho} + \frac{2\Delta\beta}{\beta}\right)\sin^2\theta + \frac{\Delta\alpha}{2\alpha}\tan^2\theta, \tag{2}$$

where $\alpha = (\alpha_1 + \alpha_2)/2$, $\rho = (\rho_1 + \rho_2)/2$, and $\beta = (\beta_1 + \beta_2)/2$. After fluid substitution in layer 2, the postproduction reflection coefficient is found to be

$$R_1^{PP}(\theta) = \frac{1}{2}\left(\frac{\Delta\rho'}{\rho'} + \frac{\Delta\alpha'}{\alpha'}\right) - \frac{2\beta'^2}{\alpha'^2}\left(\frac{\Delta\rho'}{\rho'} + \frac{2\Delta\beta'}{\beta'}\right)\sin^2\theta + \frac{\Delta\alpha'}{2\alpha'}\tan^2\theta, \tag{3}$$

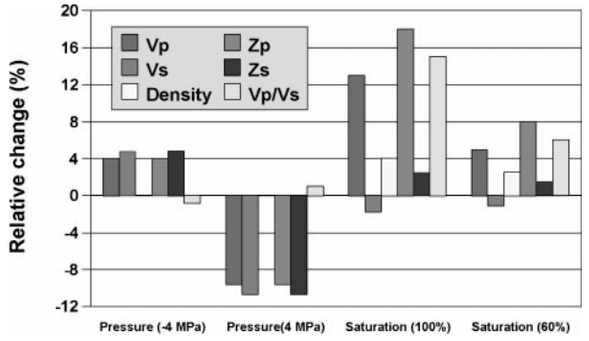

FIG. 3. Expected relative changes (%) in various seismic parameters (V_p, V_s, density, P-acoustic impedance, S-acoustic impedance and V_p/V_s ratio, from left to right for each histogram) due to changes in pore pressure and water saturation: 60% change in water saturation means from 20% to 80%; Z_p and Z_s denote P- and S-wave impedances, respectively. Average porosity is 30%, initial pore pressure is 32 MPa and the reservoir depth is approximately 2000 m. (Figure reprinted with permission from *Petroleum Geoscience*).

where

$$\Delta\alpha' = \alpha_2' - \alpha_1 = \alpha_2 + \Delta\alpha^F - \alpha_1 = \Delta\alpha + \Delta\alpha^F,$$
$$\alpha' = (\alpha_1 + \alpha_2 + \Delta\alpha^F)/2 = \alpha\left(1 + \frac{\Delta\alpha^F}{2\alpha}\right), \text{ etc.}$$

Assuming that $\Delta\alpha/\alpha \ll 1$ and $\Delta\alpha^F/\alpha \ll 1$ and neglecting higher order terms or combinations of them in either $\Delta\alpha/\alpha$ or $\Delta\alpha^F/\alpha$, we obtain

$$R_1^{PP}(\theta) = \frac{1}{2}\left(\frac{\Delta\rho}{\rho} + \frac{\Delta\alpha}{\alpha}\right) - \frac{2\beta^2}{\alpha^2}\left(\frac{\Delta\rho}{\rho} + \frac{2\Delta\beta}{\beta}\right)\sin^2\theta + \frac{\Delta\alpha}{2\alpha}\tan^2\theta + \frac{1}{2}\left(\frac{\Delta\rho^F}{\rho} + \frac{\Delta\alpha^F}{\alpha}\right) - \frac{2\beta^2}{\alpha^2}\left(\frac{\Delta\rho^F}{\rho} + \frac{2\Delta\beta^F}{\beta}\right)\sin^2\theta + \frac{\Delta\alpha^F}{2\alpha}\tan^2\theta. \tag{4}$$

In the above derivation, the following approximation for the velocity ratio term has been used:

$$\frac{\beta'}{\alpha'} = \frac{\beta\left(1 + \frac{\Delta\beta^F}{2\beta}\right)}{\alpha\left(1 + \frac{\Delta\alpha^F}{2\alpha}\right)} \approx \frac{\beta}{\alpha}. \tag{5}$$

The delta terms in this velocity ratio ($\Delta\beta^F/2\beta$, $\Delta\alpha^F/2\alpha$) are to be multiplied with other delta terms inside the brackets of equations (4) ($\Delta\rho/\rho + 2\Delta\beta/\beta$), but since they will give second-order terms they can be neglected. A detailed derivation including second-order terms can be found in Landrø (2001). Furthermore, for fluid substitution one can assume that the shear modulus remains constant, meaning that the $\sin^2\theta$-term in equations (4) does not change under fluid substitution. This can be seen in the following way: keeping the shear modulus constant means that $\beta^2\rho$ is constant, leading to the result that $\Delta\rho^F/\rho + 2\Delta\beta^F/\beta = 0$ for fluid substitution. For fluid substitution, equation (4) therefore reads

$$R_1^{PP}(\theta) \approx R_0(\theta) + \frac{1}{2}\left(\frac{\Delta\rho^F}{\rho} + \frac{\Delta\alpha^F}{\alpha}\right) + \frac{\Delta\alpha^F}{2\alpha}\tan^2\theta, \tag{6}$$

which again means that the change in reflectivity (to the lowest order) due to fluid saturation change in layer 2 is

$$\Delta R^{PP;F}(\theta) \approx \frac{1}{2}\left(\frac{\Delta\rho^F}{\rho} + \frac{\Delta\alpha^F}{\alpha}\right) + \frac{\Delta\alpha^F}{2\alpha}\tan^2\theta. \tag{7}$$

A numerical example testing the differences between using this approximate expression for reflectivity changes and using the "exact" equations shows a deviation in reflectivity of 4% at zero incidence angle and 1% at an angle of 30° (Landrø, 2001).

For pressure changes, it is reasonable to assume that the density remains practically unchanged. Assume that the bulk

density can be written as

$$\rho = \phi\rho_f + (1-\phi)\rho_s, \tag{8}$$

where ϕ is the porosity, and ρ_f and ρ_s are the fluid and matrix densities, respectively. For a sandstone reservoir, the changes in porosity due to pressure changes are generally small, and hence the changes in density due to pressure changes are also negligible. This is confirmed by the core measurement results shown in Figure 3. A corresponding equation for the reflectivity change due to a change in the pore pressure (P) can therefore be approximated (again to the lowest order) by

$$\Delta R^{PP;P}(\theta) = \frac{1}{2}\frac{\Delta\alpha^P}{\alpha} - \frac{4\beta^2}{\alpha^2}\frac{\Delta\beta^P}{\beta}\sin^2\theta + \frac{\Delta\alpha^P}{2\alpha}\tan^2\theta. \tag{9}$$

The previous analysis considered PP data only, we can extend the same analysis to PS data. A reasonable approximation (assuming weak contrasts and small angles) for the PS-reflection coefficient can be obtained from Aki and Richards (1980):

$$R_0^{PS}(\theta) = -\frac{1}{2}\left((1+2K)\frac{\Delta\rho}{\rho} + 4K\frac{\Delta\beta}{\beta}\right)\sin\theta + K\left(\left(K+\frac{1}{2}\right)\left(\frac{\Delta\rho}{\rho}+2\frac{\Delta\beta}{\beta}\right) - \frac{K}{4}\frac{\Delta\rho}{\rho}\right)\sin^3\theta, \tag{10}$$

where $K = \beta/\alpha$ denotes the V_s to V_p ratio. In order to obtain full consistency between equations (9) and (10), we should choose $\tan^2\theta \approx \sin^2\theta$ [corresponding to the small angle approximation made in equation (10)] in equation (9). However, for the current examples, we have chosen to keep equation (9) as it is. Calculating the same changes in the PS reflection coefficient as for the PP reflection coefficient yields

$$\Delta R^{PS;F}(\theta) = -\frac{1}{2}\frac{\Delta\rho^F}{\rho}\sin\theta - \frac{K^2}{4}\frac{\Delta\rho^F}{\rho}\sin^3\theta,$$
$$\Delta R^{PS;P}(\theta) = -2K\frac{\Delta\beta^P}{\beta}\sin\theta + 2K\left(K+\frac{1}{2}\right)\frac{\Delta\beta^P}{\beta}\sin^3\theta. \tag{11}$$

A reasonable assumption for the relative variation of the seismic parameters with respect to fluid saturation and effective pressure changes can be written (using first-order expansion with respect to saturation changes and second order with respect to pressure changes):

$$\frac{\Delta\alpha_2}{\alpha_2} \approx k_\alpha\Delta S + l_\alpha\Delta P + m_\alpha\Delta P^2,$$
$$\frac{\Delta\beta_2}{\beta_2} \approx k_\beta\Delta S + l_\beta\Delta P + m_\beta\Delta P^2,$$
$$\frac{\Delta\rho_2}{\rho_2} \approx k_\rho\Delta S, \tag{12}$$

where ΔS and ΔP denote the changes in oil saturation and effective pressure, respectively. Parameters $k_\alpha, k_\beta, k_\rho, l_\alpha, l_\beta, m_\alpha$, and m_β, are empirical parameters estimated from, for instance, the saturation change curve in Figure 1 and the pressure change curve in Figure 2. It should be noted that the assumptions given in equations (12) are reasonable approximations for Gullfaks field. For other fields with different reservoir properties, more advanced approximations might be necessary (e.g. Meadows, 2001). These parameters will generally be spatially variant. In practice however, it is impossible to measure these parameters at all positions in space. Therefore, a realistic approach would be to estimate one parameter set for each formation, or to assume that one average parameter set is representative for the whole field. As an example, the relative P-wave velocity increase (based on the average curve as shown in Figure 2) due to a pore pressure decrease of 4 MPa was estimated to be 4% with a standard deviation of 1.5% (corresponding to an uncertainty of 40%). The standard deviation was computed on the basis of all 29 core samples used in the Gullfaks study.

The total change in reflectivity due to the combined effect of fluid and pressure changes can thus be written:

$$\begin{aligned}\Delta R^{PP} \approx{}& \frac{1}{2}\left(k_\rho\Delta S + k_\alpha\Delta S + l_\alpha\Delta P + m_\alpha\Delta P^2\right)\\ &+ \frac{1}{2}\left(k_\alpha\Delta S + l_\alpha\Delta P + m_\alpha\Delta P^2\right)\tan^2\theta\\ &- 4K^2\left(l_\beta\Delta P + m_\beta\Delta P^2\right)\sin^2\theta,\\ \Delta R^{PS} \approx{}& -\frac{1}{2}k_\rho\Delta S\sin\theta - \frac{K^2}{4}k_\rho\Delta S\sin^3\theta - 2K\left(l_\beta\Delta P\right.\\ &\left.+ m_\beta\Delta P^2\right)\sin\theta + 2K\left(K+\frac{1}{2}\right)\left(l_\beta\Delta P\right.\\ &\left.+ m_\beta\Delta P^2\right)\sin^3\theta.\end{aligned} \tag{13}$$

For differencing time-lapse seismic data, the most robust method is to work on stacked sections (Andorsen and Landrø, 2000). Hence, equations (13) need to be integrated over a given angle span (see Appendix A). After integration, we have

$$\begin{aligned}\Delta R^{PP} \approx{}& \frac{1}{2}\left(k_\rho\Delta S + k_\alpha\Delta S + l_\alpha\Delta P + m_\alpha\Delta P^2\right)i_0\\ &+ \frac{1}{2}\left(k_\alpha\Delta S + l_\alpha\Delta P + m_\alpha\Delta P^2\right)i_3\\ &- 4K^2\left(l_\beta\Delta P + m_\beta\Delta P^2\right)i_2,\end{aligned} \tag{14}$$

$$\begin{aligned}\Delta R^{PS} \approx{}& -\frac{1}{2}k_\rho\Delta S i_1 - \frac{K^2}{4}k_\rho\Delta S i_4 - 2K\left(l_\beta\Delta P\right.\\ &\left.+ m_\beta\Delta P^2\right)i_1 + 2K\left(K+\frac{1}{2}\right)\left(l_\beta\Delta P\right.\\ &\left.+ m_\beta\Delta P^2\right)i_4,\end{aligned} \tag{15}$$

where i_0–i_4 are given in Appendix A. Rearranging these terms gives

$$\Delta R^{PP} \approx a_1\Delta S + a_2\Delta P + a_3\Delta P^2,$$
$$\Delta R^{PS} \approx b_1\Delta S + b_2\Delta P + b_3\Delta P^2, \tag{16}$$

where the coefficients are given by

$$a_1 = \frac{1}{2}k_\rho i_0 + \frac{1}{2}k_\alpha i_0 + \frac{1}{2}k_\alpha i_3,$$
$$a_2 = \frac{1}{2}l_\alpha i_0 + \frac{1}{2}l_\alpha i_3 - 4K^2 l_\beta i_2,$$
$$a_3 = \frac{1}{2}m_\alpha i_0 + \frac{1}{2}m_\alpha i_3 - 4K^2 m_\beta i_2,$$
$$b_1 = -\frac{1}{2}k_\rho i_1 - \frac{K^2}{4}k_\rho i_4,$$
$$b_2 = -2Kl_\beta i_1 + 2K\left(K + \frac{1}{2}\right)l_\beta i_4,$$
$$b_3 = -2Km_\beta i_1 + 2K\left(K + \frac{1}{2}\right)m_\beta i_4. \qquad (17)$$

Assuming that ΔR^{PP} and ΔR^{PS} can be estimated from stacked marine multicomponent time-lapse seismic data (well calibration prior to the differencing is essential), equations (14) and (15) can be solved for saturation and pressure changes, giving

$$\Delta P = \frac{\frac{b_2}{b_1}a_1 - a_2 \pm \sqrt{\left(a_2 - \frac{b_2}{b_1}a_1\right)^2 - 4\left(a_3 - \frac{b_3}{b_1}a_1\right)\left(\frac{a_1}{b_1}\Delta R^{PS} - \Delta R^{PP}\right)}}{2\left(a_3 - \frac{b_3}{b_1}a_1\right)} \qquad (18)$$

and

$$\Delta S = \frac{\Delta R^{PP} - \frac{a_3}{b_3}\Delta R^{PS} - \left(a_2 - \frac{b_2}{b_3}a_3\right)\Delta P}{a_1 - \frac{b_1}{b_3}a_3}. \qquad (19)$$

SYNTHETIC DATA EXAMPLE

Simple synthetic models with two layers were generated to test the validity of the methodology for the combination of PP and PS time-lapse data. In the synthetic models, the rock physical properties of the cap rock layer and the layer below the reservoir zone have been kept constant, and only the parameters of the reservoir rock have been changed. The reservoir rock is assumed to be buried at 2000-m depth, and the initial properties are taken from a well in Gullfaks field in the North Sea. The basic rock and fluid properties are given in Table 1. The relationship between the seismic parameters and pressure were found through statistical analysis of ultrasonic measurements from dry cores of various formations (Figure 2). The seismic parameters for different scenarios for saturated reservoir rock were then calculated using Gassmann's equation (Figure 4).

Table 1. Initial rock and fluid parameters.

Water Salinity	3.5%
Density of oil	880 kg/m^3
GOR (Gas Oil Ratio)	90
Density of gas	0.76 kg/m^3
Temperature	72°C
Initial effective pressure	6 MPa

Reflection coefficients have been calculated using Zoeppritz' equations for angles from 0° to 45°, for the different reservoir models. The reflection coefficients have been convolved with a wavelet extracted from PP seismic data from Gullfaks field, calibrated to the reflection coefficients and stacked (for angles 0–45° for PP data, and either 0–45° or 15–45° for PS data) for the different models. Figure 5 shows the PP and PS prestack synthetic seismograms for a scenario with water saturation 10% and effective pressure 6 MPa, and Figure 6 shows the same synthetic seismograms with noise added. Figure 7 shows stacked traces (0–45°) for PP and PS seismic data for the preproduction scenario described above, and a postproduction scenario with water saturation 50% and effective pressure 8 MPa. The time-lapse differences between the stacked data for PP and PS seismic are also shown.

The parameters describing the relationship between changes in seismic properties and saturation and pressure changes were estimated through statistical analysis of all the models with initial effective pressure 6 MPa and a positive water saturation change. The estimated relationships are given by

$$\frac{\Delta\alpha_2}{\alpha_2} \approx 0{,}12\Delta S + 0{,}0121\Delta P - 0{,}005\Delta P^2,$$
$$\frac{\Delta\beta_2}{\beta_2} \approx -0{,}015\Delta S + 0{,}0196\Delta P - 0{,}0021\Delta P^2,$$
$$\frac{\Delta\rho_2}{\rho_2} \approx 0{,}0293\Delta S. \qquad (20)$$

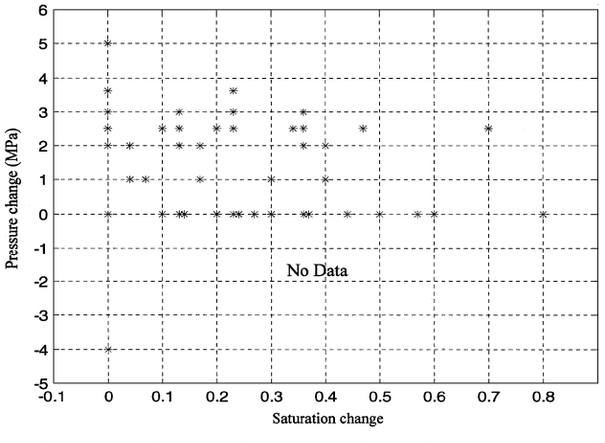

FIG. 4. Change in saturation versus change in pressure for all models (initial pressure is 6 MPa).

Using equations (20), and assuming $V_p/V_s = \alpha/\beta = 2$ (for the models tested, the V_p/V_s ratio varies between 1.92 and 2.15), equation (16) give the following relationship between the change in reflectivity and the change in saturation and pressure:

$$\Delta R^{PP} \approx 0{,}0715\Delta S - 0{,}0387\Delta P + 0{,}0043\Delta P^2,$$
$$\Delta R^{PS} \approx -0{,}0066\Delta S - 0{,}0078\Delta P + 0{,}000835\Delta P^2. \quad (21)$$

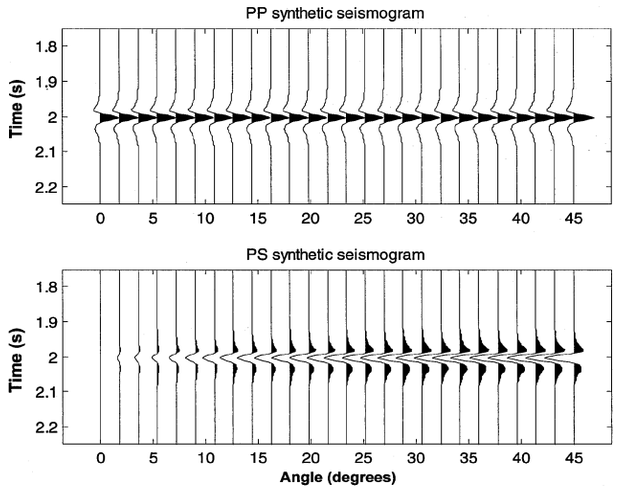

FIG. 5. Baseline synthetic seismograms for PP and PS reflections (angle gather) for a model with initial pressure 6 MPa and 10% initial water saturation.

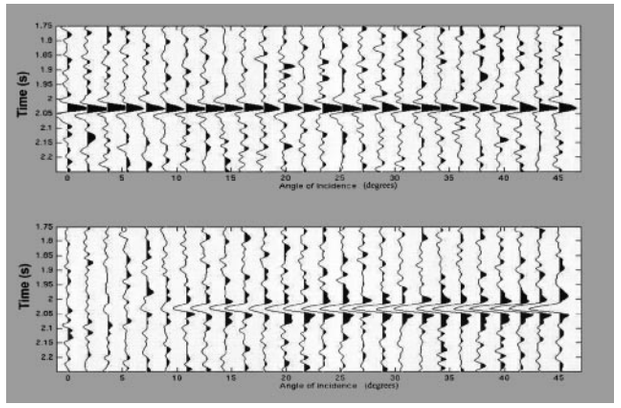

FIG. 6. Baseline synthetic seismograms for PP and PS reflections (angle gather) with noise for a model with initial pressure 6 MPa, and 10% initial water saturation.

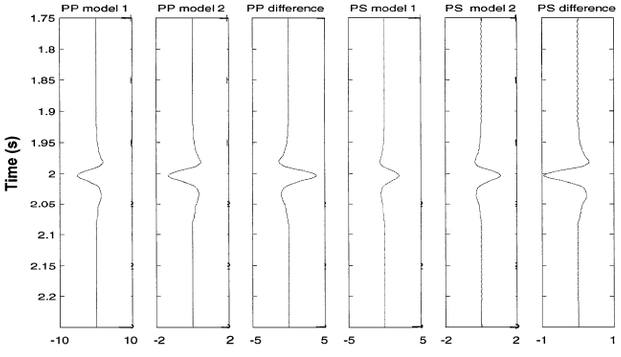

FIG. 7. Stacked traces for PP and PS reflections (angle gather) for initial model, time-lapse model, and the difference (time-lapse model – initial model).

Pairs of two models representing preproduction and postproduction stages have been analyzed to estimated the pressure and saturation changes from the seismic data. Differences between preproduction and postproduction scenarios were computed for both PP and PS data, and the estimated changes in effective pressure and saturation were calculated using equations (21).

For the example given in Figures 5–7 (line 2 in Table 2), the initial effective pressure was 6 MPa and the initial water saturation was 10%. The PP and PS data for this example were stacked from 0–45°. After production, the effective pressure was 8 MPa and the water saturation was 50%, giving $\Delta S = 0.4$ and $\Delta P = 2$ MPa. By using equations (21), the pressure change was estimated to be 1.68 MPa, and the saturation difference was estimated to be 0.34. This gives an error of 16% for the pressure change estimate, and 15% for the saturation change estimate.

Figure 6 shows a plot of the same initial model with random noise added to the gathers. The signal-to-noise ratio (SNR) is approximately 0.1 for both PP data and PS data. With this noise level, the pressure change was estimated to be 1.75 MPa, and the saturation change estimated to be 0.33. This gives an error of 12.5% for the pressure change estimate and 17.5% for the saturation change estimate. Table 2 shows the results for ten different production scenarios. Table 3 shows the estimated change in saturation and effective pressure for the same production scenarios used in Table 2, but using only time-lapse PP AVO data, as in Landrø (2001). The production changes estimated from multicomponent data are overall better than the estimations using PP AVO data alone, however, the estimated change in effective pressure has improved the most. In average, we find that the deviation in estimated saturation changes for the PP-PS-method described in this paper is 8% and 0.3 MPa for the estimated pore pressure changes. For the PP AVO method, we find that the corresponding average errors are 9% (saturation change) and 1.0 MPa (pressure change). In a second noise test, the SNR level was reduced to 0.4 (the results are listed in the last column of Table 2). The average errors for the PP-PS-method were then 12% for saturation changes and 1.3 MPa for pressure changes.

In addition to a noise sensitivity test, the reflection coefficient used to calibrate the seismic amplitudes were perturbated by perturbing the velocity and density model. Table 4 shows the results for three different perturbations: 10% increase of velocities and densities for both the preproduction and the postproduction model, 10% decrease of the velocities and density of the preproduction model only, and finally 10% increase in the velocities and densities of the preproduction model and 5% increase of the velocities and density of the postproduction model. The estimated changes in saturation are stable to the reflection coefficient perturbations, but the pressure estimates have lower quality.

Finally, a test was done with different stacking angles for the PP and PS data to investigate if the removal of the weak

amplitudes around zero offset on the PS data would improve the results. The PP data were stacked from 0–45° as before, whereas the PS data were stacked from 15° to 45° in angle of incidence. This test was performed to study the impact of offset range on the PS data with a low SNR (PS amplitudes are zero at zero offset and generally weak in amplitude for small incidence angles; therefore, the lowest SNRs ratios will occur for low offsets). For data with noise, the results were not as good as for the case where the same stacking angles were used for both PP and PS data, although the differences were small.

CONCLUSIONS

Approximate formulas for computation of saturation- and pressure-related changes from time-lapse PP and PS stacked seismic data have been derived and successfully tested on synthetic data. The formulas are explicit expressions related to PP and PS stacks and are, therefore, well suited for direct implementation in a processing package or a seismic interpretation system. Necessary input to obtain the equations is a rock physics model that relates changes in the seismic parameters to changes in pressure and saturation.

The method was tested for ten production scenarios, representing various degrees of saturation and pressure changes. It discriminates reasonably well between fluid saturation changes and pore pressure changes for most cases. A regression technique was used to build empirical rock physics relations between the seismic parameters and the fluid and pressure saturation parameters. For one scenario that was outside the database

Table 2. Estimation of saturation and effective pressure changes from 4D-4C seismic data. Sw1 and Sw2 are the saturation before and after production, and P1 and P2 are the effective pressure before and after production.

Sw1/Sw2	Real Sw Change	Est. Sw change	With noise SNR = 1	With noise SNR = 0.4	P1/P2 (MPa)	Real P Change (MPa)	Est. P change (MPa)	With noise SNR = 1	With noise SNR = 0.4
0.1/0.33	0.23	0.16	0.16	0.23	6/6	0	0.1	0.06	−2.9
0.1/0.5	0.4	0.34	0.33	0.12	6/8	2	1.68	1.75	2.5
0.1/0.6	0.5	0.41	0.39	0.47	6/6	0	0.24	0.30	−1.46
0.1/0.9	0.8	0.84	0.83	0.94	6/6	0	0.10	0.13	−2.3
0.1/0.4	0.3	0.24	0.23	0.01	6/7	1	0.88	1.06	2.8
0.33/0.4	0.07	0.08	0.07	0.1	6/7	1	0.77	0.81	2.1
0.33/0.5	0.17	0.19	0.17	0.4	6/8	2	1.55	1.52	−0.5
0.1/0.1	0	−0.30	−0.30	−0.3	6/2	−4	−3.0	−3.0	−4.3
0.1/0.7	0.6	0.52	0.50	0.3	6/6	0	0.16	0.18	−0.06
0.46/0.5	0.04	0.08	0.08	0.1	6/8	2	1.53	1.50	2.1

Table 3. Estimation of saturation and effective pressure changes from 4D PP AVO seismic data. Sw1 and Sw2 are the saturation before and after production, and P1 and P2 are the effective pressure before and after production.

Sw1/Sw2	Real Saturation Change	Estimated saturation change with noise	P1/P2 (MPa)	Real Pressure Change (MPa)	Estimated Pressure change with noise (MPa)
0.1/0.33	0.23	0.20	6/6	0	−0.29
0.1/0.5	0.4	0.46	6/8	2	0.49
0.1/0.6	0.5	0.5	6/6	0	−0.71
0.1/0.9	0.8	0.98	6/6	0	−1.4
0.1/0.4	0.3	0.31	6/7	1	0.29
0.33/0.4	0.07	0.13	6/7	1	0.28
0.33/0.5	0.17	0.27	6/8	2	0.59
0.1/0.1	0	−0.30	6/2	−4	−2.2
0.1/0.7	0.6	0.61	6/6	0	−0.13
0.46/0.5	0.04	0.16	6/8	2	0.67

Table 4. Estimation of saturation and effective pressure changes from 4D-4C seismic data with noise and reflection coefficient perturbations. A: 10% increase in V_p, V_s, and density for postpoduction and preproduction model. B: 10% decrease in V_p, V_s and density for preproduction model, no change in postproduction model. C: 10% increase in V_p, V_s, density for preproduction model and 5% increase in V_p, V_s, and density in postproduction model. Sw1 and Sw2 are the saturation before and after production, and P1 and P2 are the effective pressure before and after production.

Sw1/Sw2	Real Sw Change	Est. Sw change	A	B	C	P1/P2 (MPa)	Real P Change (MPa)	Est. P change (MPa)	A	B	C
0.1/0.33	0.23	0.16	0.15	0.16	0.16	6/6	0	0.1	0.13	0.09	0.05
0.1/0.5	0.4	0.34	0.33	0.24	0.30	6/8	2	1.68	2.35	2.14	1.92
0.1/0.6	0.5	0.41	0.32	0.31	0.46	6/6	0	0.24	−0.06	0.45	−0.05
0.1/0.9	0.8	0.84	0.93	0.79	0.86	6/6	0	0.10	0.09	0.47	−0.02
0.1/0.4	0.3	0.24	0.17	0.3	0.24	6/7	1	0.88	0.64	0.66	1.0
0.33/0.4	0.07	0.08	0.01	0.06	0.15	6/7	1	0.77	1.59	0.81	0.58
0.33/0.5	0.17	0.19	0.22	0.08	0.30	6/8	2	1.55	0.65	2.25	0.47
0.1/0.1	0	−0.30	−0.24	−0.29	−0.26	6/2	−4	−3.0	−2.68	−3.15	−3.54
0.1/0.7	0.6	0.52	0.62	0.55	0.59	6/6	0	0.16	−0.21	−0.11	0.06
0.46/0.5	0.04	0.08	0.15	0.07	0.09	6/8	2	1.53	1.6	0.54	2.2

used for the regression analysis, a large deviation in the estimated water saturation was found; for all other scenarios, the deviations between the estimated and real changes were small.

In the present method, only time-lapse amplitude changes in PP and PS are used. Use of time-lapse traveltime changes in PP and PS is probably the most promising way of reducing the uncertainties in the final saturation and pressure estimates. So far, very few real data examples (repeated marine, multicomponent data) are available, which means that the proposed algorithm has not been tested on real data.

ACKNOWLEDGMENTS

Ketil Brekke Johansen is acknowledged for performing the rock physics modeling used as a basis for the present work. The financial support through the EC ATLASS project, ENK6-CT-2000-00108, is acknowledged, as well as the ATLASS project partners: NTNU, TU Delft, CGG, Eni-Agip, Norsk Hydro, Shell, and Statoil. Helene Hafslund Veire acknowledges the support from the VISTA Ph.D. programme. Finally, the reviewers and associate editor are acknowledged for constructive reviews.

REFERENCES

Aki, K., and Richards, P., 1980, Quantitative seismology: W. H. Freeman & Co.

Andorsen, K., and Landrø, M., 2000, Source signature variations versus repeatability—A study based on a zero-offset VSP experiment: J. of Seis. Expl., **9**, 61–71.

Berg, E., Svenning, B., and Martin, J., 1994, SUMIC—A new tool for exploration and reservoir mapping: 56th Ann. Conf., Eur. Assocn. Geosci. Eng., Extended Abstracts, paper G055.

Bilgeri, D., and Ademeno, E. B., 1982, Predicting abnormally pressured sedimentary rocks: Geophys. Prosp., **30**, 608–621.

Cambois, G., 2000, Can P-wave AVO be quantitative?: The Leading Edge, **19**, 1246–1251.

Duffaut, K., Alsos, T., Landrø, M., Rogno, H., and Al-Najjar, N. F., 2000, Shear wave elastic impedance: The Leading Edge, **19**, 1222–1229.

Gabriels, P. W., Horvei, N. A., Koster, J. K., Onstein, A., and Staples, R., 1999, Time lapse seismic monitoring of the Draugen field: 69th Ann. Internat. Mtg., Soc. Explor., Geophys., Expanded Abstracts, 2035–2037.

Gassmann, F., 1951, Elastic waves through a packing of spheres: Geophysics, **16**, 673-685.

Kvam, Ø., and Landrø, M., 2001, Pressure detection from rms velocities—A sensitivity study based on a 4D dataset: 71st Ann. Internat. Mtg., Soc. Explor., Geophys., Expanded Abstracts, 1576–1579.

Landrø, M., 2001, Discrimination between pressure and fluid saturation changes from time-lapse seismic data: Geophysics **66**, 836–844.

——— 2002, Uncertainties in quantitative time-lapse seismic analysis: Geophys. Pros., **50**, 527–538.

Landrø, M., Solheim, O. A., Hilde, E., Ekren, B. O., and Strønen, L. K., 1999a, The Gullfaks 4D seismic study: Petroleum Geoscience, **5**, 213–226.

Landrø, M., Duffaut, K., and Rognø, H., 1999b, Well calibration of seabed seismic data: 69th Ann. Internat. Mtg., Soc. Explor., Geophys., Expanded Abstracts, 860–863.

MacLeod, M., Hanson, R. A., Bell, C. R., and McHugo, S., 1999, The Alba field ocean bottom cable survey: Impact on development: The Leading Edge, **18**, 1306–1312.

Meadows, M., 2001, Enhancements to Landrø's method for separating time-lapse pressure and saturation changes: 71st Ann. Internat. Mtg., Soc. Explor., Geophys., Expanded Abstracts, 1652–1655.

Reynolds, E. B., 1970, Predicting overpressured zones with seismic data: World Oil, **171**, 78–82.

Tura, A., and Lumley, D. E., 1998, Subsurface fluid-flow properties form time-lapse elastic-wave reflection data: 43rd SPIE Ann. Mtg., Mathematical Methods in Geophysical Imaging V, 125–138.

——— 1999, Estimating pressure and saturation changes from time-lapse AVO data: 69th Ann. Internat. Mtg., Soc. Explor., Geophys., Expanded Abstracts, 1655–1658.

Watts, G. F. T., Jizba, D., Gawith, D. E., and Gutteridge, P., 1996, Reservoir monitoring of the Magnus field through 4D time-lapse seismic analysis: Petroleum Geoscience, **2**, 361–372.

Winkler, K. W., 1985, Dispersion analysis of velocity and attenuation in Berea sandstone: J. Geophys. Res., **90**, 6793–6800.

APPENDIX A

INTEGRATION OVER ANGLE SPAN

For differencing time lapse seismic data, the most robust method is to work on stacked sections (Andorsen and Landrø, 2000). Hence, equation (13) need to be integrated over a given angle span, as shown below.

$$i_0 = \frac{1}{\theta_2-\theta_1}\cdot\int_{\theta_1}^{\theta_2} d\theta = 1,$$

$$i_1 = \frac{1}{\theta_2-\theta_1}\cdot\int_{\theta_1}^{\theta_2} \sin\theta d\theta = \frac{1}{\theta_2-\theta_1}(\cos\theta_1-\cos\theta_2),$$

$$i_2 = \frac{1}{\theta_2-\theta_1}\cdot\int_{\theta_1}^{\theta_2} \sin^2\theta d\theta = \frac{1}{\theta_2-\theta_1}\left(\frac{1}{2}(\theta_2-\theta_1)\right.$$
$$\left.-\frac{1}{4}(\sin 2\theta_2-\sin 2\theta_1)\right),$$

$$i_3 = \frac{1}{\theta_2-\theta_1}\cdot\int_{\theta_1}^{\theta_2} \tan^2\theta d\theta = \frac{1}{\theta_2-\theta_1}(\tan\theta_2-\tan\theta_1$$
$$-(\theta_2-\theta_1)),$$

$$i_4 = \frac{1}{\theta_2-\theta_1}\cdot\int_{\theta_1}^{\theta_2} \sin^3\theta d\theta = \frac{1}{\theta_2-\theta_1}\left(-(\cos\theta_2-\cos\theta_1)\right.$$
$$\left.=+\frac{1}{3}\left((\cos\theta_2)^2-(\cos\theta_1)^2\right)\right). \qquad \text{(A-1)}$$